J. Fetal Med. (December 2021) 8:279–291
https://doi.org/10.1007/s40556-021-00329-z

ORIGINAL ARTICLE

Diagnostic Evaluation of the Posterior Fossa with Antenatal and Post-Mortem MRI: An Unfolded View

Neetika Gupta[1] · Claudia Martinez-Rios[1] · Dina El Demellawy[2] · Nick Barrowman[3] · Elka Miller[1]

Received: 14 September 2021 / Accepted: 14 December 2021 / Published online: 8 January 2022

Abstract The role of post-mortem fetal conventional autopsy (CA) is undisputed but poses challenges with small, macerated bodies, and increasing parental refusal. Fetal post-mortem magnetic resonance imaging (PMMRI) is a less invasive alternative that can be used for assessment of the brain, including the posterior fossa (PF) structures. The purpose of this study was to evaluate the imaging characteristics of the PF in PMMRI compared to antenatal MRI (ANMRI), using CA as the gold standard. A retrospective, single-center study of ten fetuses who underwent ANMRI, PMMRI, and CA from August 2010 to May 2018. The PF structures were evaluated qualitatively for imaging findings, and quantitatively by obtaining the transcerebellar diameter, vermian length, brainstem thickness, width of the fourth ventricle and cisterna magna, skull base angles, and PF volume. Twenty MRI exams were included. The median gestational age of ANMRI was 21.7 weeks. The median age at termination of pregnancy (TOP) and PMMRI was 23.7 weeks. There was good congruence between PMMRI, ANMRI, and CA, with 60% complete congruence and 40% partial congruence between ANMRI and PMMRI. PMMRI and CA showed 70% complete congruence, and 20% partial congruence. No incongruence was noted. PF evaluation on CA was not possible in 1 case due to maceration. Quantitative evaluation in PMMRI showed significant enlargement of most PF structures compared to ANMRI and smaller CSF-filled spaces (p value < 0.05). PMMRI is an acceptable imaging modality for the macroscopic evaluation of PF structures. Smaller CSF-filled spaces and enlargement of the brain are expected findings when evaluating PMMRI.

Keywords Fetal imaging · Post-mortem MRI · Antenatal MRI · Posterior fossa · Conventional autopsy · Brain malformation

✉ Neetika Gupta
drneetika@yahoo.com

Claudia Martinez-Rios
claudiamonica@gmail.com

Dina El Demellawy
deldemellawy@cheo.on.ca

Nick Barrowman
NBarrowman@cheo.on.ca

Elka Miller
EMiller@cheo.on.ca

[1] Medical Imaging Department, CHEO, University of Ottawa, Ottawa, ON, Canada

[2] Department of Pathology and Laboratory Medicine, CHEO, Faculty of Medicine, University of Ottawa, Ottawa, ON, Canada

[3] CHEO Research Institute, Ottawa, ON, Canada

Introduction

Fetal brain malformations are one of the most common causes for termination of pregnancy (TOP) [1, 2], and posterior fossa (PF) malformations are the most common brain anomalies identified on antenatal imaging [3–6]. Intrauterine fetal imaging techniques for evaluation of the PF include ultrasound (US) as a primary imaging modality and antenatal magnetic resonance imaging (ANMRI) for further characterization of brain abnormalities [7, 8]. A precise antenatal imaging interpretation is of utmost importance and helps in deciding management, guiding genetic testing, and counseling of the parents [9]. Nonetheless, a final post-mortem (PM) diagnosis is often

requested and, traditionally it has been obtained by conventional autopsy (CA).

CA remains the gold standard for diagnosis and elucidation of antenatal findings, and to establish the cause of fetal death, in cases of fetal demise [10]. However, CA poses challenges due to the intrinsic fragility of the small fetuses, the need for fixation for adequate tissue evaluation, or technically suboptimal evaluation in the macerated fetus [11]. These difficulties, together with religious considerations and parental psychologic distress, have led to the increased refusal of consent for CA [12–14], mandating the need for an alternative and more acceptable diagnostic test for PM evaluation of fetuses.

Different imaging modalities have been used to assess the fetus in the PM period. The US offers easy access and affordability, but its limiting factors include overlapping cranial sutures and brain maceration [15]. Microfocus computed tomography (CT) has shown good results for fetuses < 20 weeks of gestational age (GA) [16–18]. However, inadequate distribution of contrast (staining), and increased "source-to-object" and "object-to-detector" distance may result in poor image resolution. PMMRI has proven to be a less invasive, relatively accurate, and more acceptable technique for the assessment of the brain in fetuses > 20 weeks GA [11, 18–22]. PMMRI is the most researched imaging technique, with a fairly high diagnostic accuracy. It has been useful even with fetal maceration, where CA may fail [11, 15, 17, 19].

Numerous physiologic changes occur after death, including tissue maceration, autolysis, and decomposition [23]. In the head, cranial shape changes with vault collapse and attenuated brain tissue contrast has been described. Familiarization with these changes, for appropriate interpretation of the imaging findings is very important [24]. In this study, we aimed to evaluate the qualitative and quantitative characteristics of the PF structures on PMMRI, and compared them to ANMRI, using CA as the gold standard. A second objective was to assess the imaging changes of the PF structures in PMMRI.

Materials and Methods

This retrospective, single-tertiary care pediatric institute study was approved by the institutional review ethics board. Informed consent was waived for the study. However, as per institutional protocol and routine clinical management, all cases were discussed with a multidisciplinary team before and after the ANMRI. Written informed consent was obtained for all PMMRI and CA. All post-mortem fetuses and tissue samples were managed as per institutional standard protocol. The fetuses did not undergo the fixation process before the PMMRI.

Patient Selection

A search of the electronic medical record (EMR) in the Medical Imaging Department was performed to identify fetuses > 20 weeks GA who underwent PMMRI, ANMRI, and CA, over an eight-year period, between 1 August 2010 to 31 May 2018. All fetuses selected met the inclusion criteria (GA > 20 weeks, ANMRI, PMMRI, and CA were done). Fetuses were excluded if no CA was available.

MR Imaging Data Acquisition

MRIs were obtained using a 1.5 Tesla (T) (GE Signa Excite HDxt) or a 3 T (Siemens MAGNETOM Skyra) MRI scanner. Imaging parameters and protocols for both magnets followed the standard institutional protocol for ANMRI and PMMRI (Table 1). No contrast or sedation was used.

Selection of Images

Every ANMRI and PMMRI study was reviewed by a pediatric radiology fellow (NG), who selected the T2-weighted sequences for the ANMRI and PMMRI. Sequences were excluded if motion artifacts or abnormal projections were noted. An acceptable axial plane demonstrated the entire cerebellum and the middle

Table 1 ANMRI and PMMRI imaging parameters and protocols

Parameters	1.5 T (ANMRI)	3 T (ANMRI)	1.5 T (PMMRI)	3 T (PMMRI)
Coil	8-channel body coil	18-channel body coil	8-channel surface coil	18-channel surface coil
T2-weighted	SSFSE	HASTE	TSE	HASTE
TR/TE	3000/87.8 ms	1400/96 ms	3200/388	2500 / 73
FOV	340	280	160	150
Slice thickness	3 mm	3 mm	3 mm	3 mm

TR Time to repeat, *TE* time to echo, *FOV* field of view, *SSFSE* Single-shot fast spin echo, *HASTE* Half-Fourier Acquisition Single-shot turbo spin echo, *FSE* fast spin echo, *TSE* turbo spin-echo

cerebellar peduncles to obtain the maximum transverse diameter, and bone-to-bone PF measurements; if this was not available, a mid-coronal plane was used. The midline sagittal plane included the corpus callosum, vermis of the cerebellum, fastigium of the vermis, and the ventral bulging of the pons in the same image. A senior neuroradiologist (EM) blinded to the patient's information, corroborated that the image selection was appropriate for the study.

Image Interpretation

All MR images were evaluated by three readers including two pediatric neuroradiologists (EM and CMR) with 19 and 6 years of experience in fetal imaging respectively, and a pediatric radiology fellow (NG). The two pediatric neuroradiologists were blinded to all clinical information, GA, and magnet strength. Before assessing the cases, the readers interpreted 5 fetal MR examinations that were randomly selected and outside of the study group, to review and reach a consensus on the definitions, evaluation of different brain structures, site and approach for measurements. All the ANMRI and PMMRI biometry was based on the gestational age-based normogram [25]. Disagreements between readers were resolved by consensus.

MRI Qualitative and Quantitative Image Assessment

The PF structures were assessed in both ANMRI (Fig. 1) and PMMRI (Fig. 2) qualitatively for morphology and imaging characteristics, and quantitatively as follows:

Posterior fossa (PF): Bone-to-bone PF diameter and PF volume, calculated manually by freehand tracing of the bony margins of the PF on the consecutive T2-weighted axial images, multiplied by the slice thickness (Figs. 1a, 2a).

Vermis: Height obtained in the midsagittal plane (Figs. 1b, 2b).

Cerebellar hemispheres: Maximum transverse diameter (TCD) obtained in the axial plane (Figs. 1c, 2c).

Brainstem: Anteroposterior measurement of the midbrain peduncles obtained in the axial plane (Figs. 1d, 2d). Thickness of the pons and medulla were obtained in the sagittal plane (Figs. 1e, 2e).

Fourth ventricle: Maximum anteroposterior diameter was obtained in the sagittal plane at the level of the fastigial point (Figs. 1e, 2e).

Cisterna magna: Maximum width was obtained between the inferior margin of the vermis and the posterior rim of the foramen magnum in the axial or sagittal planes (Figs. 1c, 2c).

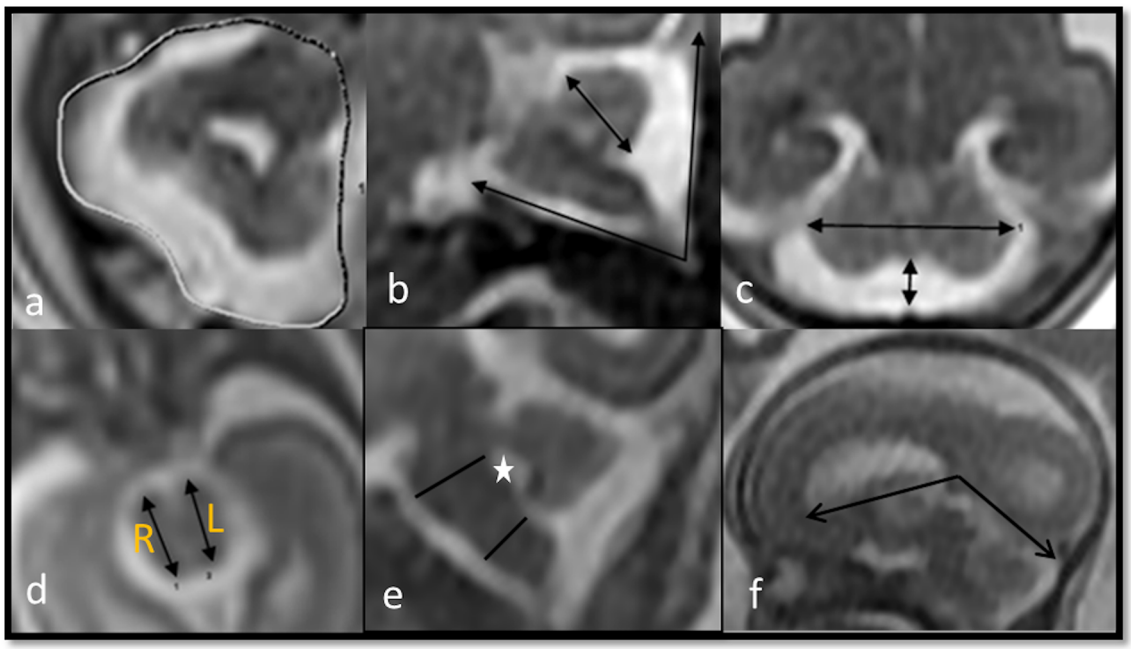

Fig. 1 PF measurements on ANMRI. Fetal T2W axial and sagittal images demonstrate: **a** freehand tracing of the bony margins of the PF on the axial image; **b** craniocaudal vermian length (arrow) and CSA on the sagittal image; **c** transverse cerebellar diameter (TCD) (long arrow) and cisterna magna (short arrow) on the axial image; **d** anteroposterior diameter of the midbrain (R – right; L – left); **e** anteroposterior diameter of pons (long line), medulla (short line) and 4th ventricle (star), and **f** the tentorial angle between bicallosal line and tentorium cerebelli

Table 2 Table showing relevant US, ANMRI, PMMRI, CA and genetics of all the fetuses

#	GA (w) ANMR	GA (w) TOP	Gap in TOP-PMMR (hrs)	US	ANMRI	PMMRI	Conventional Autopsy	Genetic	Congruence AN & PMMRI	Congruence PMMR & CA
1	25	28	6	Twin with IUGR and abnormal Doppler	No posterior fossa anomalies	No posterior fossa anomalies	No posterior fossa anomalies	−ve	C	C
2	20	21.3	10	Hydrocephalus, only one eye, cleft lip and palate	Aqueductal stenosis and severe hydrocephalus indenting on posterior fossa	Aqueductal stenosis and severe hydrocephalus indenting on posterior fossa	Aqueductal stenosis and severe hydrocephalus	+ ve AR	C	C
3	20	23.2	70	Partial agenesis of the corpus callosum Small vermis	Hypoplasia of the splenium of corpus callosum Vermis small Cerebellum unremarkable	Partial agenesis of the Corpus callosum and hippocampal commissure Small vermis and cerebellum Delayed sulcation	Agenesis of splenium of corpus callosum and hippocampal commissure Delay sulcation Posterior fossa content, does not allow a decent autopsy examination as the cerebellum was macerated	N/D	P	N/P
4	21.3	24	48	Severe IUGR, and Arnold chiari malformation (ACM)	ACM I with no obvious spinal dysraphism Cord low lying	ACM I with no obvious spinal dysraphism Cord low lying	No spinal dysraphism Cord low lying Small size of posterior fossa	−ve	C	C
5	21	22.4	72	Vermian agenesis	Severe vermian hypoplasia Cerebellar hemispheres are slightly small Borderline diminished volume of the belly of the pons,? pontocerebellar hypoplasia	Severe vermian hypoplasia Pons normal Cerebellum normal	Severe vermian hypoplasia Pons and cerebellum normal	−ve	P	C
6	22	24.1	110	IUGR and hydrocephalus	Low lying spinal cord Posterior fossa mildly crowded	Low lying cord posterior fossa appear crowded	Posterior fossa crowded Cerebellum was disproportionally small for the extent of IUGR Spinal cord was low and tethered	N/D	C	P

Table 2 continued

#	GA (w) ANMR	GA (w) TOP	Gap in TOP-PMMR (hrs)	US	ANMRI	PMMRI	Conventional Autopsy	Genetic	Congruence AN & PMMRI	Congruence PMMR & CA
7	21.1	23.3	113	Previous pregnancy with Acrocallosal syndrome	Small vermis concern for Joubert like syndrome	Small vermis No Joubert syndrome Cerebellum normal	Small vermis but no e/o Joubert No agenesis Asymmetry of the cerebellar hemispheres, the left being smaller	+ ve (SLOS) DHCR7 gene	P	P
8	22.1	23.1	47	Extrophy and IUGR	Brain small for GA, otherwise normal	Germinal matrix, trigone and choroid plexus bleed	Multifocal hemorrhage including posterior fossa	−ve	C	C
9	27.5	28.6	44	Hydrocephalus, high suspicious of porencephalic cyst	Interhemispheric (I/H) cyst, and Copus callosum agenesis (CCA) Severe mass effect and crowding of PF	I/H Cyst, CCA & severe mass effect on PF Status post cephalocentesis a left parieto-occipital defect	I/H Cyst, CCA & severe mass effect and crowding of PF Collapsed skull bone flaps following cephalocentesis prior to delivery	N/D	C	C
10	36	37.5	90	Mild ventriculomegaly Query cortical malformation development	Microcephaly Migration anomaly / heterotopia Post fossa normal and symmetrical	Microcephaly & migration anomaly/ schizencephaly Suspected band heterotopia Flattened pons and midbrain	Microcephaly, diffuse polymicrogyria, suspected heterotopias, closed lip schizencephaly Wallerian deg and hypoplastic crus of midbrain basis pontis, medulla and cord Cerebellum was small similar to cerebrum	N/D	P	C

IUGR: intrauterine growth restriction, −ve: negative, + ve: positive, P: partial congruence, C: complete congruence, N/D: not done, N/P: not possible, w: weeks, hrs: hours, AR: autosomal recessive, SLOS: Smith-Lemli-Opitz syndrome

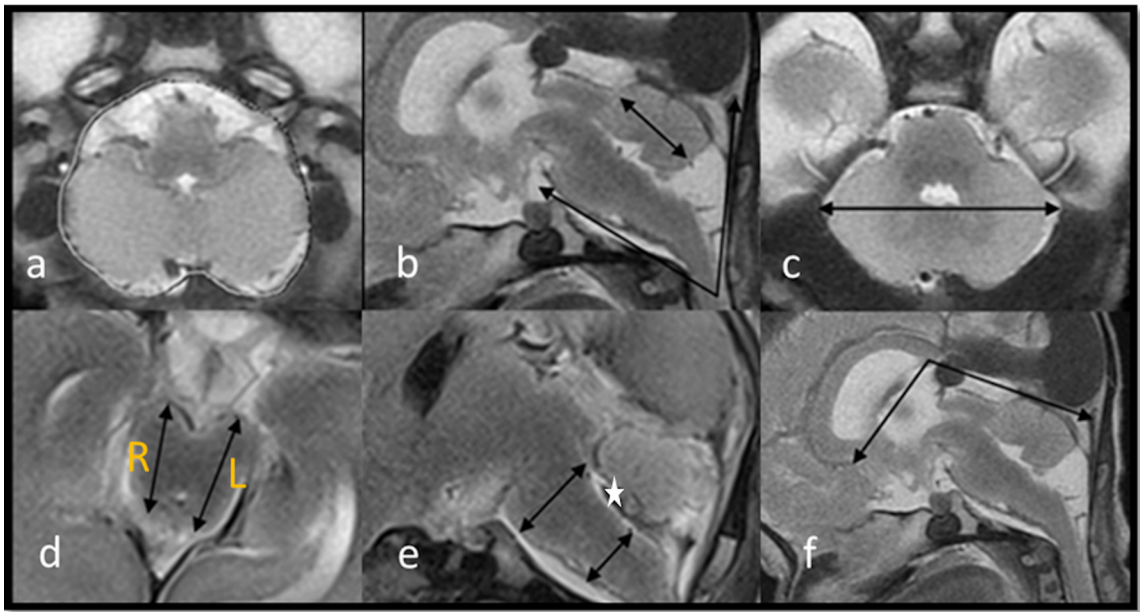

Fig. 2 PF measurements on PMMRI. T2W axial and sagittal images demonstrate: **a** freehand tracing of the bony margins of the PF on the axial image; **b** craniocaudal vermian length (arrow) and CSA on the sagittal image; **c** TCD (arrow) and effaced cisterna magna on the axial image; **d** anteroposterior diameter of the midbrain (R – right. L – left); **e** anteroposterior diameter of pons (long arrow), medulla (short arrow) and effaced 4th ventricle (star); and **f** tentorial angle between bicallosal line and the tentorium cerebelli

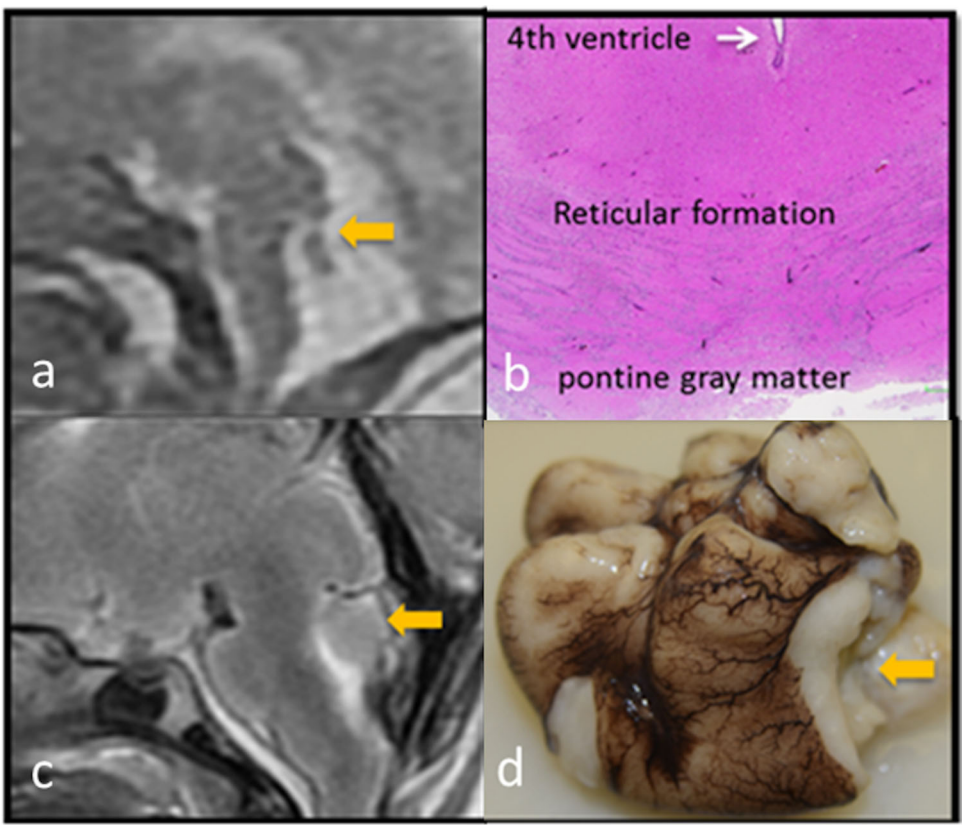

Fig. 3 *Fetus 5.* Sagittal T2W ANMRI (**a**) demonstrating a small vermis (arrow) and pons, but PMMRI (**c**) showed normal-appearing pons and hypoplastic vermis (arrow). Gross pathology (**d**), confirmed a hypoplastic vermis (arrow) with normal pons, confirmed by microscopy (**b**)

Skull base: The clival-supraoccipital angle (CSA) was measured by drawing a line along the posterosuperior surface of the clivus, connecting the most cranial part of the clivus and anterior border of basion, and by drawing a second line along the superior surface of the supraoccipital, along the anterior border of the opisthion (1b, 2b). The tentorial angle (TA) was measured by drawing a line joining the anterior and posterior aspects of the corpus callosum (bi-callosal line) and a line parallel to the tentorium cerebelli (Figs. 1f, 2f). The CSA and TA were obtained using the midsagittal T2-weighted images.

Measurements were documented in millimeters (mm) and angles in degrees. The readers' measurements and interpretations were documented individually in separate Excel worksheets (Microsoft 2016) and then merged for analysis.

Conventional Autopsy and Genetic Analysis

Both macro and microscopic pathological findings of all fetuses were collected from the report available in the EMR. The pathologist had access to the ANMRI and PMMRI reports at the time of the CA, as per standard of care. All relevant CA findings were correlated with ANMRI and PMMRI (Table 2). Genetic testing was performed at the discretion of fetal medicine specialists.

Statistical Analysis

Demographics and imaging data were documented in a Microsoft Excel sheet. The data were analyzed using the SPSS 27.0 for Windows software package (SPSS Inc.). The mean ratios of the measurements from the PMMRI against the ANMRI were estimated. To test the hypothesis that the mean ratio was 1, paired t-test was used to compare log-transformed post-mortem measurements to log-transformed fetal measurements. *P* values from these tests were adjusted for multiple comparisons using Holm's method and 95% confidence intervals for the mean ratio were obtained by exponentiating the lower and upper confidence limits for the difference in means.

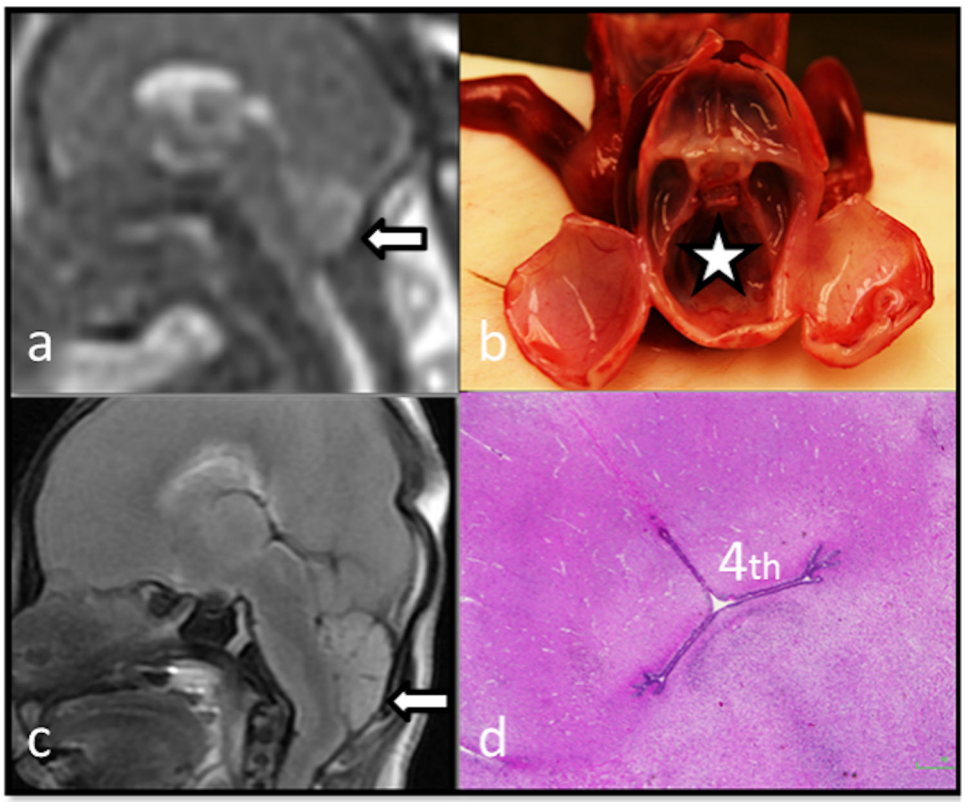

Fig. 4 *Fetus 4.* ANMRI (**a**) and PMMRI (**c**) sagittal T2W images show complete congruence for Chiari I malformation (arrow), confirmed by the gross pathological examination (**b**) showing funneling of the posterior fossa (star), and low power microscopy (**d**) showing an effaced fourth ventricle

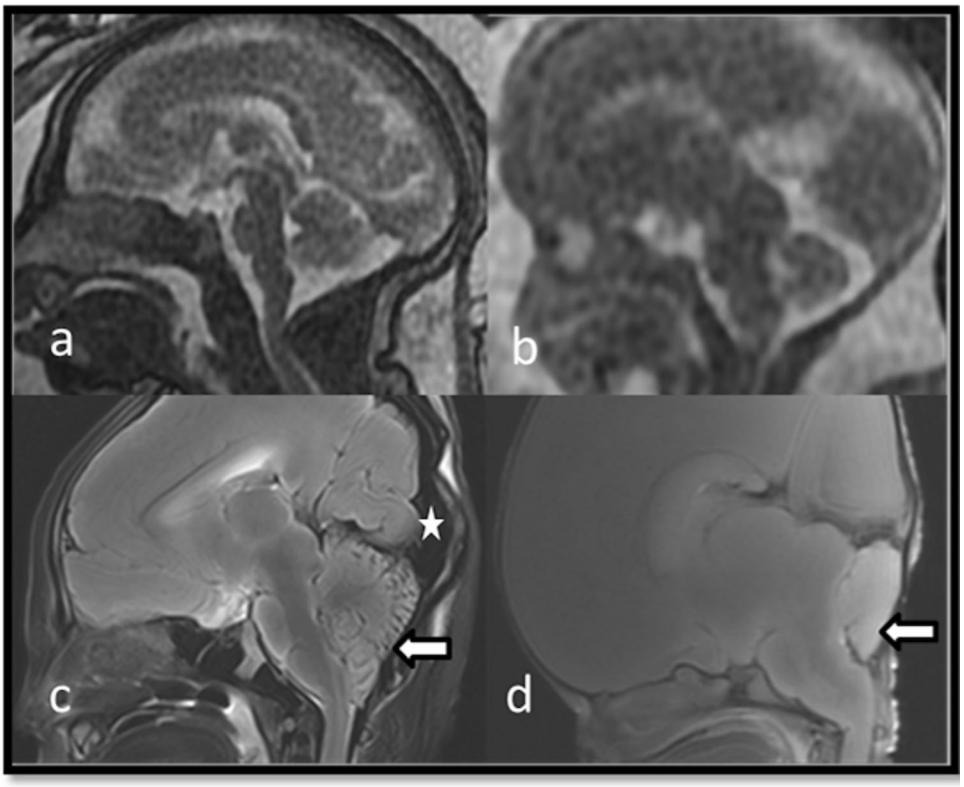

Fig. 5 Expected mild physiological cranial collapse with crowding of PF structures noted resulting in physiological tonsillar herniation (arrow) in sagittal T2W PMMRI (**c**, **d**) compared to ANMRI (**a**, **b**). Note the prominent venous sinuses (star) on (**c**), also a physiologic PMMRI change from venous stasis

Results

Patients

Twenty MRI exams (10 antenatal and 10 post mortem) from ten patients were included. The median GA at ANMRI was 21.7 weeks (interquartile range of 21.0 – 23.5 weeks). All TOPs were performed by induction of labor and vaginal delivery, except for one fetus. Fetus 9 was delivered by cesarean section, due to a large interhemispheric cyst and hydrocephalus requiring intrapartum cephalocentesis. All fetuses underwent PMMRI and CA within 1–5 days of TOP. The median age at TOP and PMMRI was 23.7 weeks (interquartile range of 23.2–27.0 weeks). The median time gap between ANMRI and PMMRI was 2.2 weeks (interquartile range of 1.6–2.5 weeks.) The median time gap between TOP and PMMRI was 60 h (interquartile range of 48–90 h).

Qualitative Imaging Assessment

Fetal abnormalities included vermian hypoplasia (Fig. 3), cerebellar hypoplasia and asymmetry, and small PF with Chiari malformation (Fig. 4). One fetus also showed microcephaly with small PF and multiple supratentorial abnormalities including commissural agenesis, abnormal, delayed sulcation, migration anomalies (polymicrogyria, schizencephaly, heterotopias). One fetus had a large interhemispheric cyst and hydrocephalus. Attenuated brain tissue contrast with edema and venous stasis was seen in all PMMRI. Inferior cerebellar herniation (Fig. 5) is a physiological finding found in the post-mortem period.

When comparing PMMRI with ANMRI, there was complete congruence in 6/10 fetuses and partial congruence in 4/10 fetuses. The reasons for partial congruence included the inability of ANMRI to detect cerebellar hypoplasia in *fetus 3* and a brainstem abnormality in *fetus 10*. For *fetus 5,* possible pontine hypoplasia was suspected on ANMRI, but not in the PMMRI. *Fetus 7* had a small vermis and was suspected of Joubert syndrome, but genetic testing confirmed Smith-Lemli-Opitz syndrome. *Fetus 1* was part of monochorionic twin pregnancy with severe IUGR and was concerning for cortical malformation on ultrasound and ANMRI but normal appearing posterior fossa. The PMMRI was done only for IUGR fetus with cortical malformation.

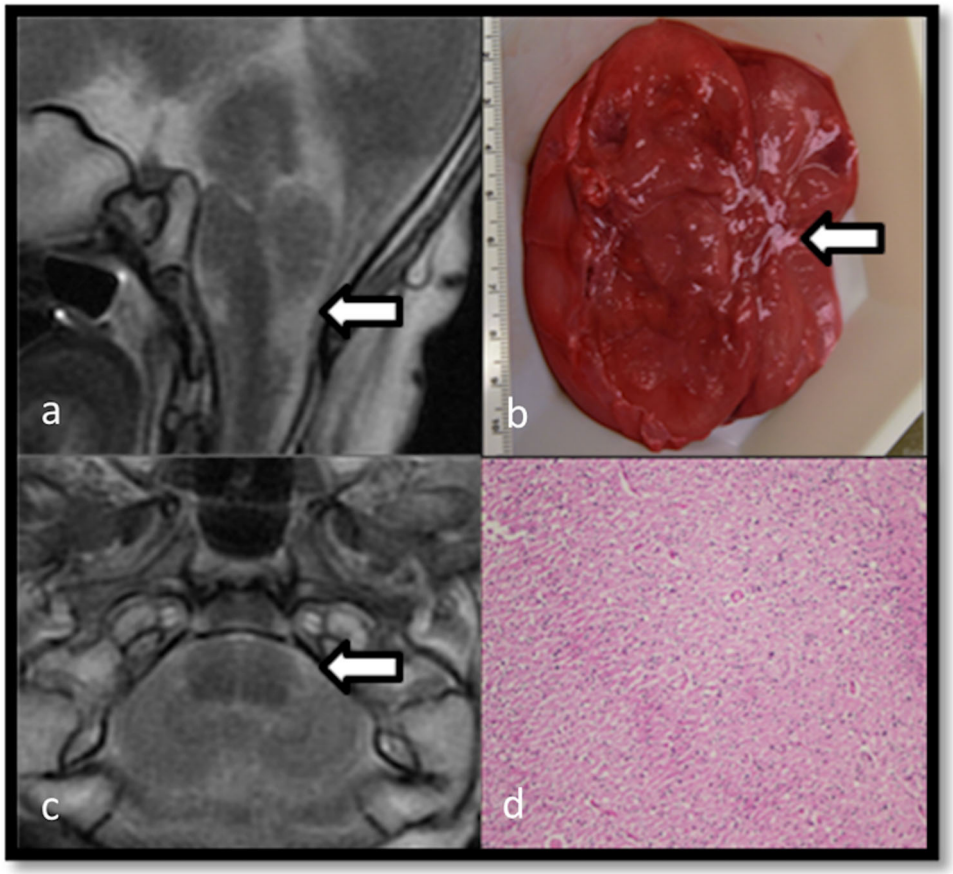

Fig. 6 *Fetus 3.* Sagittal (**a**) and axial (**c**) T2W PMMRI can appreciate and differentiate the PF structures into brainstem, cerebellum and vermis. Gross examination on CA (**b**) was challenging due to severe maceration and inability to differentiate PF structures. Even histology was difficult to interpret due to liquefaction and cell destruction (**d**)

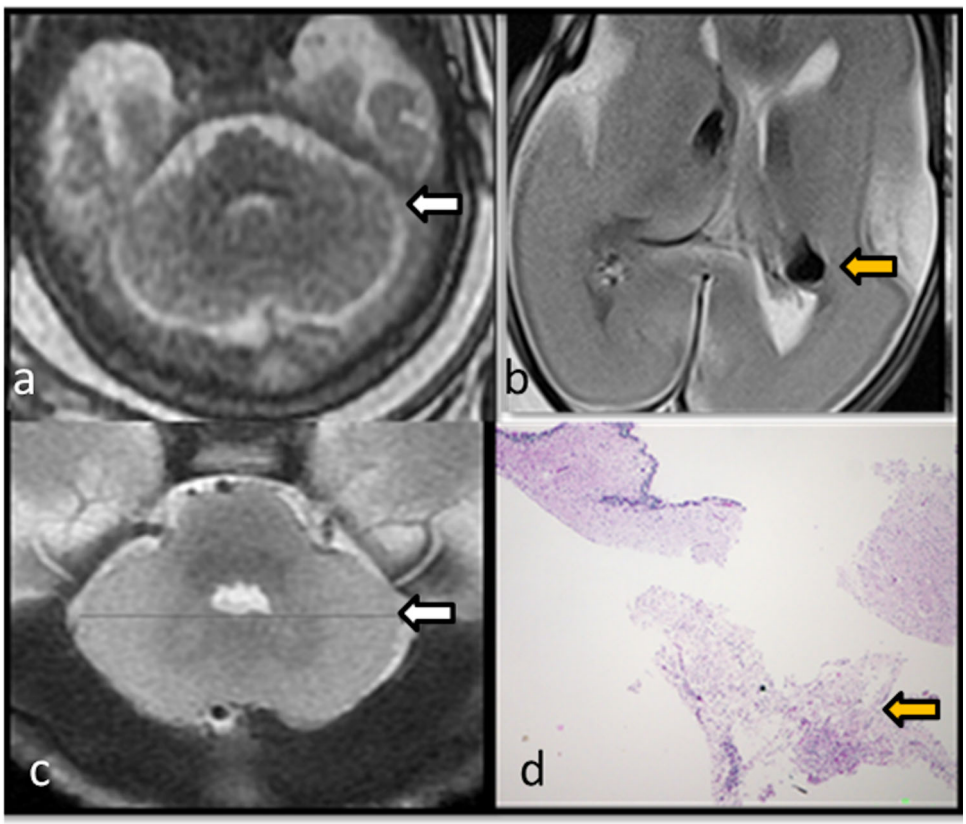

Fig. 7 Physiological enlargement of parenchyma, loss of grey-white matter differentiation and decreased CSF-spaces (white arrows) on axial T2W PMMRI (**c**) compared to ANMRI (**a**). There is also mild intraventricular hemorrhage (yellow arrows) on axial T2W PMMRI (**b**) confirmed by microscopy (**d**)

Comparing PMMRI with CA, there was good congruence, with complete congruence noted in 7 fetuses and partial congruence in 2 out of the 10 fetuses. The partial congruence was for a small cerebellum in *fetus 6* and asymmetric cerebellum in *fetus 7* missed on PMMRI but described on the CA. Of note, *fetus 6* had crowding of the neural structures in the PF, limiting assessment on PMMRI. For *fetus 7*, a small vermis and cerebellum were identified in ANMRI and PMMRI, but no asymmetry was noted. Finally, *fetus 3* showed a small cerebellum and vermis on ANMRI but the assessment of PF structures with CA was not possible due to maceration (Fig. 6); however, the PMMRI allows the assessment of the PF structures despite the maceration. No incongruence was noted.

Quantitative Imaging Assessment

PMMRI showed statistically significant enlargement of parenchymal PF structures (Figs. 7 and 8) ranging between 19% to 25% ($p < 0.05$) compared with ANMRI, except for the thickness of the medulla, where the adjusted p value ($p \sim 0.19$) was not statistically significant. The PF CSF-filled spaces (Figs. 7 and 8) showed a statistically significant decrease in size ($p < 0.05$) compared to ANMRI. For example, the cisterna magna showed a mean percentage decrease in size of 69% and the fourth ventricle of 26%. The PF volume, bone-to-bone PF diameter and clival-supratentorial angle showed no statistically significant change in size (adjusted p value > 0.05). The mean ratio, confidence interval, and p value of all the parameters are presented in Table 3 and Fig. 8.

Conventional Autopsy and Genetic Analysis

CA of the PF structures was possible in nine fetuses. In all cases, photographs of the external and salient internal examination findings were taken as standard institutional CA protocol. CA of the PF was not possible in one fetus due to severe maceration. Four fetuses underwent further dedicated neuropathological examination. Genetic testing was performed in 6 fetuses with positive results in 2 of them: *fetus 7* with DHCR7 gene mutation (Smith-Lemli-Opitz syndrome) and *fetus 2* with a non-specific autosomal recessive mutation.

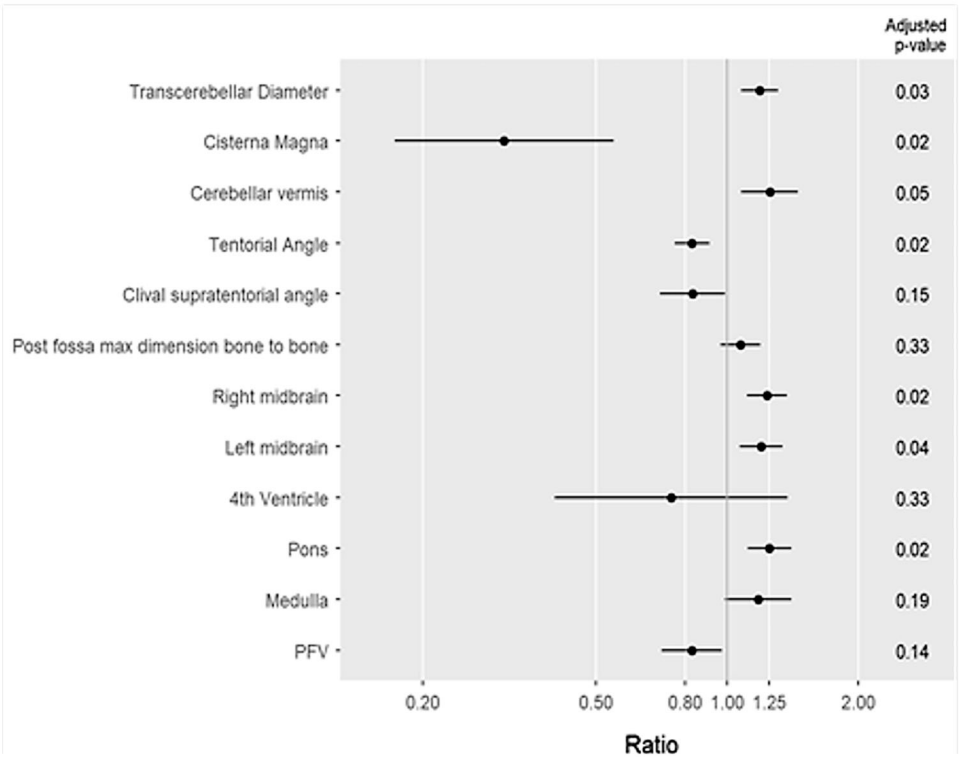

Fig. 8 Ratios of PF structure measurements on PMMRI. The central line represents the value of 1 (PMMRI ~ ANMRI), PMMRI parameters on the right side of the line measures less than ANMRI and on the left side measures more than ANMRI. Statistically significant decrease in size noted in cisterna magna and fourth ventricle with increase in size of TCD, vermis and brainstem structures

Table 3 Mean ratio, confidence interval and *p* value of quantitative parameters

Parameters	Mean ratio	95% CI	*p* value	p. adjusted
Transcerebellar Diameter	1.19	1.08, 1.31	0.003	0.03
Cisterna Magna	0.31	0.17, 0.55	0.001	0.02
Cerebellar vermis	1.25	1.08, 1.45	0.01	0.05
Tentorial Angle	0.83	0.76, 0.91	0.001	0.02
Clival supratentorial angle	0.83	0.70, 0.99	0.04	0.15
Post fossa bone-bone diam	1.07	0.97, 1.19	0.17	0.33
Right midbrain	1.23	1.11, 1.37	0.002	0.02
Left midbrain	1.20	1.07, 1.34	0.01	0.04
4th Ventricle	0.74	0.40, 1.38	0.30	0.33
Pons	1.25	1.11, 1.40	0.002	0.02
Medulla	1.18	0.99, 1.40	0.06	0.19
PF volume	0.83	0.71, 0.97	0.03	0.14

Mean ratio of the parameters on PMMRI compared to the ANMRI. The value > 1 suggests an increase in the size and < 1 decrease in size. The adjusted p valve < 0.05 suggests change is statistically significant

CI Confidence Interval

Discussion

We evaluated the imaging characteristics of PMMRI compared to ANMRI in the assessment of the PF structures with CA. Our study showed good congruence of the PMMRI findings when compared to the ANMRI and CA in the assessed fetuses. Similarly, Izzo G et al. [26] and Goergen SK et al. [27] demonstrated high concordance between ANMRI and PMMRI in detecting fetal brain abnormalities, contributing to the CA findings. Goergen SK et al. also emphasized the fact that both ANMRI and PMMRI should not be assessed independent to each other and highlighted that reliance on PMMRI alone, may result in misdiagnosis [27]. Advantages of PMMRI are its non-invasiveness and relative ease to perform the examination without the need for tissue preparation, compared to CA. Also, macroscopic changes secondary to delivery, death, and maceration can be assessed on imaging.

In our cohort, the PF structures were appropriately characterized on ANMRI and PMMRI for most fetuses along with CA except for one fetus, where CA evaluation was non-diagnostic due to severe maceration. However, ANMRI and PMMRI showed near complete congruence of the findings and we found that PMMRI was decisive and even superior to CA in one case (*fetus 3*). Similarly, Shruthi et al. [19], found that PMMRI was comparable and even superior to CA for PF abnormalities. Authors also found that PMMRI can provide additional diagnostic information of the fetal nervous system and can be an acceptable alternative to CA when this is refused by the parents [11, 15, 17, 19].

To our knowledge, this is the first study assessing the PF structures on PMMRI both subjectively and objectively, compared to ANMRI; keeping CA as gold standard. In our study, PMMRI demonstrated brain edema with loss of grey-white matter differentiation, diffuse enlargement of most solid PF brain structures, and smaller CSF-filled spaces, as has been described in the literature. [28] These changes are due to post-mortem altered CSF dynamics and CSF redistribution into the brain parenchyma resulting in cell changes that appears similar to the cerebral edema from antenatal/perinatal ischemic injury, an expected post-mortem finding that should not be mistaken for pathology [28]. The CSF redistribution causes brain enlargement (swelling), poor grey-white matter differentiation, venous stasis, and effacement of extra-axial CSF spaces together with skull deformity and collapse [29]. An apparent tonsillar descent (Fig. 5) due to cerebellar swelling can occur and should not be considered a pathological finding (e.g. Chiari 1 malformation) [23]. Montaldo et al., quantified the post-mortem body changes secondary to maceration using whole-body fetal PMMRI compared to CA, and developed a PMMRI-based scoring system [30]. The authors found a good correlation between the PMMRI-based maceration score and the extent of maceration seen on CA. They found that a decrease in brain tissue contrast strongly correlated with the extent of maceration, and concluded that this maceration score could be useful when interpreting the PMMRI (30).

Limitations of this study include its retrospective nature, small sample size, limited spectrum of PF abnormalities, and relatively wide range of gestational age of our cohort. There might be a selection bias since the MRI studies were performed for fetuses with suspected brain abnormalities. Not all fetuses underwent dedicated neuropathological examination or genetic testing, and for one fetus assessment of PF structures by CA was not possible. Despite this, the study provides a window of opportunity for further

larger-size, multi-institutional prospective studies with broader PF or brain pathology, including AN/PMMRI, using CA as a reference standard, and incorporating parental opinions to enable this post mortem fetal assessment approach as an evidence-based practice.

Conclusion

PMMRI is an effective tool for the evaluation of PF structures and complements ANMRI and CA. It is advantageous by avoiding the disfigurement of the fetus from tissue manipulation and processing seen with CA.

PF brain enlargement and smaller CSF-filled spaces are expected post-mortem physiological phenomenon and need to be taken into consideration when reporting PMMRI.

References

1. Vaknin Z, Lahat Y, Barel O, Ben-Ami I, Reish O, Herman A, Maymon R. Termination of pregnancy due to fetal abnormalities performed after 23 weeks' gestation: analysis of indications in 144 cases from a single medical center. Fetal Diagn Ther. 2009;25(2):291–6. https://doi.org/10.1159/000229501 (**Epub 2009 Jul 24 PMID: 19628945**).
2. Aslan H, Yildirim G, Ongut C, Ceylan Y. Termination of pregnancy for fetal anomaly. Int J Gynaecol Obstet. 2007;99(3):221–4. https://doi.org/10.1016/j.ijgo.2007.05.047 (**Epub 2007 Sep 24 PMID: 17889880**).
3. Adamsbaum C, Moutard ML, André C, Merzoug V, Ferey S, Quéré MP, Lewin F, Fallet-Bianco C. MRI of the fetal posterior fossa. Pediatr Radiol. 2005;35(2):124–40. https://doi.org/10.1007/s00247-004-1316-3 (**Epub 2004 Nov 23 PMID: 15565345**).
4. Limperopoulos C, du Plessis AJ. Disorders of cerebellar growth and development. Curr Opin Pediatr. 2006;18:621–7.
5. Garel C. New advances in fetal MR neuroimaging. Pediatr Radiol. 2006;36(7):621–5. https://doi.org/10.1007/s00247-006-0200-8 (**Epub 2006 May 3 PMID: 16770666**).
6. Limperopoulos C, Robertson RL Jr, Khwaja OS, Robson CD, Estroff JA, Barnewolt C, Levine D, Morash D, Nemes L, Zaccagnini L, du Plessis AJ. How accurately does current fetal imaging identify posterior fossa anomalies? AJR Am J Roentgenol. 2008;190(6):1637–43. https://doi.org/10.2214/AJR.07.3036.PMID:18492918;PMCID:PMC2692250.
7. Van Doorn M, Oude Rengerink K, Newsum EA, Reneman L, Majoie CB, Pajkrt E. Added value of fetal MRI in fetuses with suspected brain abnormalities on neurosonography: a systematic review and meta-analysis. J Matern Fetal Neonatal Med. 2016;29(18):2949–61. https://doi.org/10.3109/14767058.2015.1109621 (**Epub 2015 Nov 23 PMID: 26592136**).
8. Rossi AC, Prefumo F. Additional value of fetal magnetic resonance imaging in the prenatal diagnosis of central nervous system anomalies: a systematic review of the literature. Ultrasound Obstet Gynecol. 2014;44(4):388–93. https://doi.org/10.1002/uog.13429 (**Epub 2014 Aug 21 PMID: 24890732**).
9. Batty R, Gawne-Cain ML, Mooney C, Mandefield L, Bradburn M, Mason G, Griffiths PD. Analysis of errors made on in utero MR studies of the foetal brain in the MERIDIAN study. Eur Radiol. 2019;29(1):195–201. https://doi.org/10.1007/s00330-018-5508-x (**Epub 2018 Jun 15. PMID: 29948083; PMCID: PMC6291426**).
10. Coady AM, Bower S. Fetal Pathology. In Twining's Textbook of Fetal Abnormalities (3rd edn). Churchil Livingstone: London, 2014.
11. Arthurs OJ, Thayyil S, Pauliah SS, Jacques TS, Chong WK, Gunny R, Saunders D, Addison S, Lally P, Cady E, Jones R, Norman W, Scott R, Robertson NJ, Wade A, Chitty L, Taylor AM, Sebire NJ. Magnetic resonance imaging autopsy study (MaRIAS) collaborative group. diagnostic accuracy and limitations of post-mortem MRI for neurological abnormalities in fetuses and children. Clin Radiol. 2015;70(8):872–80. https://doi.org/10.1016/j.crad.2015.04.008 (**Epub 2015 Jun 6. PMID: 26050535**).
12. Shojania KG, Burton EC. The vanishing nonforensic autopsy. N Engl J Med. 2008;358(9):873–5. https://doi.org/10.1056/NEJMp0707996 (**PMID: 18305264**).
13. Cronin RS, Li M, Wise M, Bradford B, Culling V, Zuccollo J, Thompson JMD, Mitchell EA, McCowan LME. Late stillbirth post mortem examination in New Zealand: Maternal decision-making. Aust N Z J Obstet Gynaecol. 2018;58(6):667–73. https://doi.org/10.1111/ajo.12790 (**Epub 2018 Mar 5 PMID: 29505671**).
14. Thayyil S, Sebire NJ, Chitty LS, Wade A, Chong W, Olsen O, Gunny RS, Offiah AC, Owens CM, Saunders DE, Scott RJ, Jones R, Norman W, Addison S, Bainbridge A, Cady EB, Vita ED, Robertson NJ, Taylor AM; MARIAS collaborative group. Post-mortem MRI versus conventional autopsy in fetuses and children: a prospective validation study. Lancet. 2013 20;382(9888):223–33. https://doi.org/10.1016/S0140-6736(13)60134-8. Epub 2013 May 16. Erratum in: Lancet. 2013 Dec 14;382(9909):1980. Erratum in: Lancet. 2013;382(9888):208. PMID: 23683720.
15. Shelmerdine SC, Sebire NJ, Arthurs OJ. Diagnostic accuracy of postmortem ultrasound vs postmortem 1.5-T MRI for non-invasive perinatal autopsy. Ultrasound Obstet Gynecol. 2021;57(3):449–58. https://doi.org/10.1002/uog.22012 (**PMID: 32149428**).
16. Hutchinson JC, Kang X, Shelmerdine SC, Segers V, Lombardi CM, Cannie MM, Sebire NJ, Jani JC, Arthurs OJ. Postmortem microfocus computed tomography for early gestation fetuses: a validation study against conventional autopsy. Am J Obstet Gynecol. 2018;218(4):445.e1-445.e12. https://doi.org/10.1016/j.ajog.2018.01.040 (**Epub 2018 Feb 2 PMID: 29410108**).
17. Kang X, Cannie MM, Arthurs OJ, Segers V, Fourneau C, Bevilacqua E, Cos Sanchez T, Sebire NJ, Jani JC. Post-mortem whole-body magnetic resonance imaging of human fetuses: a comparison of 3-T vs. 1.5-T MR imaging with classical autopsy. Eur Radiol. 2017;27(8):3542–53. https://doi.org/10.1007/s00330-016-4725-4 (**Epub 2017 Jan 23. PMID: 28116518**).
18. Kang X, Carlin A, Cannie MM, Sanchez TC, Jani JC. Fetal postmortem imaging: an overview of current techniques and future perspectives. Am J Obstet Gynecol. 2020;223(4):493–515. https://doi.org/10.1016/j.ajog.2020.04.034 (**Epub 2020 May 4 PMID: 32376319**).
19. Shruthi M, Gupta N, Jana M, Mridha AR, Kumar A, Agarwal R, Sharma R, Deka D, Gupta AK, Kabra M. Conventional vs virtual autopsy with postmortem MRI in phenotypic characterization of stillbirths and fetal malformations. Ultrasound Obstet Gynecol. 2018;51(2):236–45. https://doi.org/10.1002/uog.17468 (**PMID: 28295775**).
20. Ashwin C, Hutchinson JC, Kang X, Langan D, Jones R, Norman W, Cannie M, Jani J, Sebire NJ, Arthurs OJ. Learning effect on perinatal post-mortem magnetic resonance imaging reporting: single reporter diagnostic accuracy of 200 cases. Prenat Diagn.

2017;37(6):566–74. https://doi.org/10.1002/pd.5043 (**Epub 2017 May 23 PMID: 28342279**).
21. Kang X, Sanchez TC, Arthurs OJ, Bevilacqua E, Cannie MM, Segers V, Lecomte S, Sebire NJ, Jani JC. Postmortem fetal imaging: prospective blinded comparison of two-dimensional ultrasound with magnetic resonance imaging. Ultrasound Obstet Gynecol. 2019;54(6):791–9. https://doi.org/10.1002/uog.20217 (**PMID: 30644623**).
22. Shelmerdine SC, Arthurs OJ, Gilpin I, Norman W, Jones R, Taylor AM, Sebire NJ, Chitty LS. Is traditional perinatal autopsy needed after detailed fetal ultrasound and post-mortem MRI? Prenat Diagn. 2019;39(9):818–29. https://doi.org/10.1002/pd.5448 (**Epub 2019 Apr 15 PMID: 30892705**).
23. Arthurs OJ, Barber JL, Taylor AM, Sebire NJ. Normal perinatal and paediatric postmortem magnetic resonance imaging appearances. Pediatr Radiol. 2015;45(4):527–35. https://doi.org/10.1007/s00247-014-3166-y (**Epub 2015 Apr 1. PMID: 25828356; PMCID: PMC4381098**).
24. Genest DR, Williams MA, Greene MF. Estimating the time of death in stillborn fetuses: I. Histologic evaluation of fetal organs; an autopsy study of 150 stillborns. Obstet Gynecol. 1992;80(4):575–84 (**PMID: 1383898**).
25. In Kline-Fath, B. M., In Bahado-Singh, R., & In Bulas, D. I. (2015). Fundamental and advanced fetal imaging: Ultrasound and MRI.
26. Izzo G, Talenti G, Falanga G, Moscatelli M, Conte G, Scola E, Doneda C, Parazzini C, Rustico M, Triulzi F, Righini A. Intrauterine fetal MR versus postmortem MR imaging after therapeutic termination of pregnancy: evaluation of the concordance in the detection of brain abnormalities at early gestational stage. Eur Radiol. 2019;29(6):2740–50. https://doi.org/10.1007/s00330-018-5878-0 (**Epub 2018 Dec 12 PMID: 30542750**).
27. Goergen SK, Alibrahim E, Govender N, Stanislavsky A, Abel C, Prystupa S, Collett J, Shelmerdine SC, Arthurs OJ. Diagnostic assessment of foetal brain malformations with intra-uterine MRI versus perinatal post-mortem MRI. Neuroradiology. 2019;61(8):921–34. https://doi.org/10.1007/s00234-019-02218-9 (**Epub 2019 May 10. PMID: 31076826; PMCID: PMC6620257**).
28. Offiah CE, Dean J. Post-mortem CT and MRI: appropriate post-mortem imaging appearances and changes related to cardiopulmonary resuscitation. Br J Radiol. 2016;89(1058):20150851. https://doi.org/10.1259/bjr.20150851 (**Epub 2015 Nov 12. PMID: 26562099; PMCID: PMC4985223**).
29. Victoria T, Capilla E, Chauvin NA, Johnson AM, Kramer SS, Epelman M. MR evaluation of fetal demise. Pediatr Radiol. 2011;41(7):884–9. https://doi.org/10.1007/s00247-011-1995-5 (**Epub 2011 Mar 8 PMID: 21384261**).
30. Montaldo P, Addison S, Oliveira V, Lally PJ, Taylor AM, Sebire NJ, Thayyil S, Arthurs OJ. Quantification of maceration changes using post mortem MRI in fetuses. BMC Med Imaging. 2016;27(16):34. https://doi.org/10.1186/s12880-016-0137-9. PMID:27121379;PMCID:PMC4849089.